The International Journal of Advanced Manufacturing Technology (2019) 102:1153–1163
https://doi.org/10.1007/s00170-018-2947-0

ORIGINAL ARTICLE

A new trochoidal pattern for slotting operation

Zhaoyu Li[1] · Ke Xu[2] · Kai Tang[1]

Received: 20 June 2018 / Accepted: 29 October 2018 / Published online: 6 November 2018

Abstract
Slotting is a common machining operation in manufacturing. Trochoidal milling is a good strategy for slotting, owing to its reduced cutting force load and better heat dissipation, which help significantly prolong the tool service life. Nevertheless, the traditional circular type trochoidal milling suffers from a longer total machining time due to its unfavorable chip removal rate. As an improvement to this quandary, a new type of trochoidal pattern is proposed in this paper, which is applicable to an arbitrary complex slot with a curved boundary and varying width. This new type is more flexible to adjust, unlike the conventional circular type whose adjustment margin is severely limited. Then, towards the objective of minimizing the total machining time, optimization is performed to find the best tool path of the new trochoidal pattern for the given slot, subject to the given threshold on the maximum cutter-workpiece engagement angle which is *the* key to gauge the heat dissipation and cutting force. Both computer simulations and physical cutting experiments are conducted and the results have confirmed the intended advantages of the proposed new type of trochoidal pattern over the traditional circular type.

Keywords Trochoidal milling · Machining efficiency · Tool path optimization · Slotting · Engagement angle

1 Introduction

Slotting is a popular means for initiating a rough milling process such as pocketing. Typically, there are two popular tool path patterns for a slotting process: contour parallel and direction parallel [1]. These two patterns typically require a full (cutter-workpiece) engagement angle, resulting in a larger cutting force, the worsened heat dissipation problem, as well as the accelerated tool wear, especially when cutting hard materials such as Ni-Ti alloy. Intuitively, people intend to avert these issues by reducing the feed rate and limiting the material removal rate (MRR), while the machining efficiency is degraded. Cutters equipped with super hard materials are also adopted for slotting super alloys [2], but with only marginal improvement.

Therefore, in the era of high speed machining (HSM), trochoidal tool path is becoming more and more popular for slotting and pocketing operation. Traditional trochoidal tool path can be viewed as a combination of a cyclic circular motion and a linear motion [3, 4]. By adopting the trochoidal trajectory, the full-engagement situation can be avoided upon a proper selection of step distance [5]. Trochoidal milling has recently gained its popularity in corner machining [6–8]; also, added with its better dynamics, it is now widely used in cutting hard materials, like NiTi-based super alloy [9–11]. Additionally, there are also plenty of work about trochoidal tool path planning for pocket milling, such as references [12–14].

As cyclic as the trochoidal milling is supposed to be, the cutting force changes periodically during the milling process. Various studies on cutting force-related subjects in trochoidal machining have been reported. A detailed analysis on trochoidal milling was made by Otkur and Lazoglu [4], in which the change of engagement angle was analyzed and a cutting force model was established. In reference [15], Pleta et al. built a cutting force analysis model based on the real cutting chip thickness, which can be used to analyze more complex trochoidal trajectories. Kardes and Altintas [16] established a model of mechanics and dynamics for the circular type trochoidal milling process, introducing a way to lower the chatter and improve the machining stability.

✉ Kai Tang
mektang@ust.hk

[1] Hong Kong University of Science and Technology, Hong Kong, China

[2] Nanjing University of Aeronautics and Astronautics, Nanjing, China

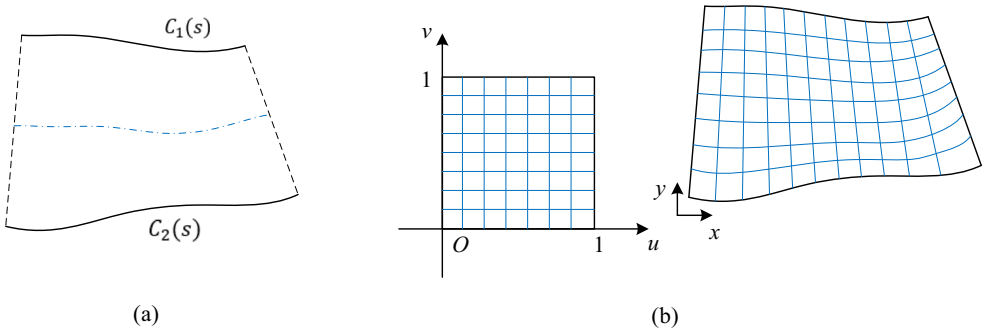

Fig. 1 **a** Geometric representation of a slot; **b** parameterization of the slot

As is well known, trochoidal milling is superior for its reduced cutting force load; however, its supremacy is mostly attributed to high-speed machining, where very high spindle speed and feed rate are attainable. When it comes to conventional machining with limited spindle speed and feed rate, trochoidal milling is never among the top choices for high efficiency. To improve its efficiency, people have tried to find a better combination of machining parameters such as cutting depth, cutting speed, and feed rate [17, 18]. Aside from the machining efficiency, these parameters were also investigated by Rauch et al. [3] for enhancing the stability and safety of trochoidal milling. Furthermore, to increase the MRR, from the perspective of machining stability, a method for optimizing the step distance of trochoidal milling was proposed by Yan et al. [19]. Wang et al. [20] presented an adaptive method for trochoidal milling, in which the radius of circular trochoidal tool path was adjusted to fit into the given complex pocket, and the step distance was also adjusted accordingly to maintain a relatively stable cutting depth and MRR. Some other perspectives for trochoidal milling optimization were also suggested. Salehi et al. [21] proposed an epicycloidal tool path milling strategy, whose trajectory is the combination of two trochoidal motions. A novel milling-milling strategy and its realizing mechanism were proposed by Li et al. [22], in which the cutter holder was designed to hold several cutters to perform a trochoidal trajectory. The MRR can be improved markedly with this method but with limited applications.

All of the above research works target at raising the efficiency of trochoidal milling by adjusting various machining parameters or finding their best combination. However, none of them ever attempted to optimize the shape of the cyclic trochoidal curve itself. In trochoidal milling, within each cutting cycle, the engagement angle varies between zero and a maximum, whereas only in a very small portion of the cycle is the engagement angle near the maximum. Therefore, the average value of engagement angle is much lower than the maximum, dragging down the MRR and hence the machining efficiency. This situation will never get resolved if the trochoidal curve maintains its circular form.

Motivated by the above prescribed problem, in this paper, we present a new type of trochoidal tool path for cutting an arbitrary slot with a curved boundary and varying width. Basically, unlike the conventional circular type, for our new type, the basic trochoidal curve is not an arc but a polynomial curve that is adjusted adaptively towards the objective of minimizing the total machining time, subject to the constraint of a given maximum engagement angle. More specifically, for an arbitrary slot, the total length of our new type of trochoidal tool path will always be shorter than that of the traditional circular type, while both respecting the given threshold on the engagement angle. Our computer simulation as well as physical cutting tests have confirmed this and validated the effort.

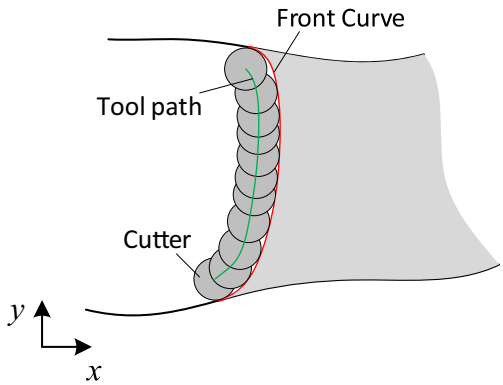

Fig. 2 Front curve and tool path

2 Spline-based trochoidal pattern

To cut a 2D slot (or simply slot), compared to the traditional circular trochoidal pattern, the new spline-based trochoidal pattern to be presented next strives to maximize the average cutter-workpiece engagement angle towards the specified threshold and hence improve the MRR (i.e., the cutting efficiency). But first of all, we need to give a concise representation of a general slot.

2.1 Parameterization of an arbitrary slot

Any slot can be fully described by its upper and lower boundary curve. In order to standardize the mathematical formulation to facilitate our new trochoidal pattern generation, we establish a parametric transformation between any slot and a unit square of parametric domain, as follows.

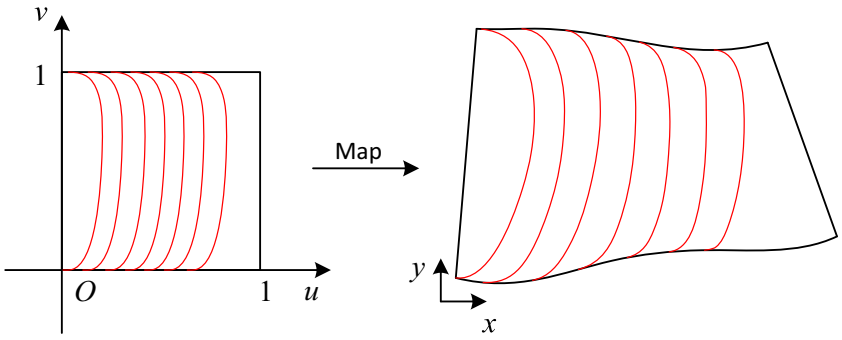

Fig. 3 Mapping front curves from the parameter domain to the object domain

Refer to Fig. 1a, the upper and lower boundary curve of the slot are $C_1(u)$ and $C_2(u)$, respectively. As we are dealing with a slot which by default is long and hence the shapes of its two ends are insignificant, we can assume that the two ends are simply line segments. Therefore, the slot can be represented by the ruled surface between the two boundary curves, i.e., Eq. (1) below:

$$r(u,v) = (1-v)C_1(u) + vC_2(u) \tag{1}$$

Obviously, this is a one-to-one mapping. In addition, as $C_1(u)$ and $C_2(u)$ are assumed to be regular and at least twice differentiable, the tangent condition is well preserved from the parametric domain to the object domain. Specifically, if any two C^1 curves σ_1 and σ_2 in the uv domain are tangent to each other at a point p, then, their images $r(\sigma_1)$ and $r(\sigma_2)$ must be tangent to each other at point $r(p)$. This property will be fully exploited by us to optimize the shape of the front curve. But first, a formal description of the front curve in slot machining is given next.

2.2 Definition of the front curves

During a slot cutting process, the envelope profile formed by the moving cutter during each engaging cycle is referred as the *front curve*, as shown in Fig. 2, where the green curve is the trajectory of the cutter's center, namely, the tool path. Geometrically, the front curve is simply the (self-interference removed) offset curve of the cutter by the cutter's radius, and vice versa. Apparently, the front curve fully determines the profile of the in-process slot, which in turn directly affects the subsequent cutting process. Therefore, the entire slot cutting process can be represented by a series of advancing front curves and our objective is to find such a series that will result in a shorter total machining time (with respect to a constant feed rate) while subject to the maximum engagement angle threshold.

We note that a better front curve should have the following two properties in order to achieve a higher machining efficiency. First, the corresponding tool path should be short. Secondly, with respect to the current front curve, the next one should advance as far as possible, as long as the engagement angle does not exceed the threshold. Because our slot is a general one with varying width and curved boundary curves, we are facing a global optimization problem; that is, two locally optimal adjacent front curves might well be inferior in terms of the final total machining time. To make it computationally feasible, we adopt the following optimization strategy: while front curves could be all different from each other, their inverse images in the uv parametric domain are identical copies that are placed along the u-axis with variable step-over distances, as illustrated in Fig. 3. Let us refer to these inverse image curves as uv-front curves. While the displacement between each two neighboring uv-front curves is yet to be determined, let us first give a mathematical description of the uv-front curves.

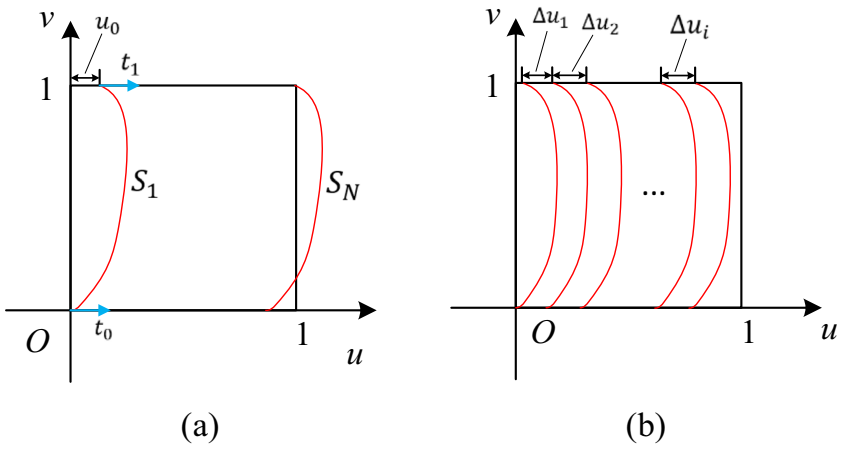

Fig. 4 **a** The first and last uv-front curve S_1 and S_N; **b** the sequence of uv-front curves

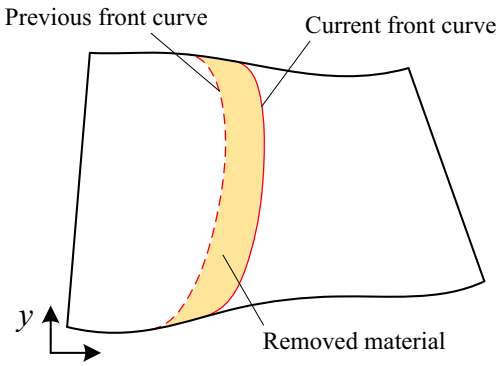

Fig. 5 The material to be removed between two consecutive front curves

We use the cubic spline to represent a *uv*-front curve. Consider the very first *uv*-front curve S_1: while it must start at (0, 0) (since, as assumed, the cutting starts at the lower-left corner of the slot), it does not have to end at (0, 1) (note that, as this is a slot cutting, the cutting time spent at the two ends is negligible to that spent in the main body of the slot). However, because every front curve must be co-tangent with the boundary curves of the slot, the tangents at the two ends of every *uv*-front curve must be along the *u*-axis. So, as illustrated in Fig. 4a, let the three scalars $\{u_0, t_0, t_1\}$ define S_1, where u_0 defines the horizontal position of the end point, whereas t_0 and $t_1$specify the magnitudes of tangents at the two end points. Mathematically, we have the following equation:

$$S_1 : \begin{cases} u_1(s) = t_0 s + (3u_0 - 2t_0 + t_1)s^2 + (-2u_0 + t_0 - t_1)s^3 \\ v_1(s) = 3s^2 - 2s^3 \end{cases} \quad s \in [0, 1] \tag{2}$$

Let $S_i(s) = \{u_i(s), v_i(s)\}$ $(i = 1, 2, \ldots, N)$ denote the sequence of *uv*-front curves, starting from S_1 and ending at S_N for some N yet to be determined. We impose that for the last *uv*-front curve S_N, it must end at (1, 1) in the *uv*-domain, as shown in Fig. 4a. Because all the *uv*-front curves are assumed to have an identical shape, as shown in Fig. 4b, letting Δu_i be the displacement between S_i and S_{i+1}, S_i then is related to S_1 by the following equation:

$$S_i : \begin{cases} u_i(s) = u_1(s) + \sum_{j=1}^{j=i-1} \Delta u_j \\ v_i(s) = 3s^2 - 2s^3 \end{cases} \quad s \in [0, 1] \tag{3}$$

Let $F_i = r(S_i)(i = 1, 2, \ldots)$ denote the sequence of corresponding front curves in the slot. Our task now becomes to find proper values for the parameters $\{t_0, t_1, u_0, u_1, u_2, \ldots\}$ so that, when the last front curve $F_N$reaches the end of the slot for some N, the total length of the tool path of the N front curves is the shortest while the maximum engagement angle constraint is respected between any consecutive front curves F_i and F_{i+1} for $i = 1, 2, \ldots, N\text{-}1$.

3 Optimization of the front curves

3.1 Treatment of the maximum engagement angle constraint

As shown in Fig. 5, the region sandwiched between the previous and current front curve, i.e., F_i and F_{i+1}, is exactly the material removed by the cutter along the tool path of the current front curve F_{i+1}. Obviously, to shorten the total machining time and also to advance the cutter as far as possible, a larger Δu_i is preferred. However, as illustrated in Fig. 6, a larger Δu_i also induces a larger engagement angle which must be capped under a given threshold.

Let θ_{i_max} denote the maximum engagement angle when cutting the $(i+1)^{\text{th}}$ chip, namely, the material between the front curves F_i and F_{i+1}. Once the current *uv*-front curve S_i is known, as all the *uv*-front curves have the same shape, if Δu_i is also determined, so is S_{i+1} and F_{i+1}, and hence the maximum engagement angle θ_{i_max} between F_i and F_{i+1}. In particular, we will use Δu_{i_max} to denote the Δu_i that will make θ_{i_max} reach the given maximum engagement angle threshold θ_s. To calculate Δu_{i_max}, we offer two simple strategies: the uniform distribution and the sequential maximization, as elaborated next.

3.1.1 Uniform Δu_i

In this simple strategy, all the $\Delta u_i's$ are the same for $i = 1, 2, \ldots, N$. In other words, the *uv*-front curves $S_i's$ are uniformly distributed along the *u*-axis; that is, $S_i = S_1 + (i-1)\Delta u_c$ for

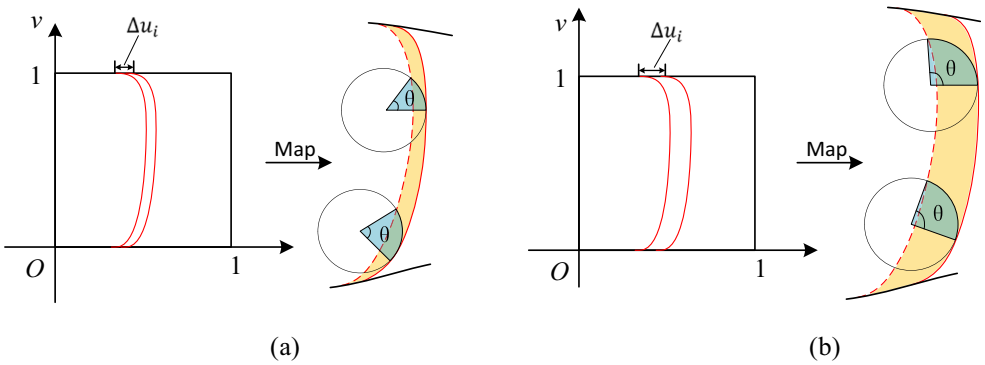

Fig. 6 The maximum engagement angle between F_i and F_{i+1}, is proportional to the displacement Δu_i

some constant Δu_c. Letting Propagation_Constant_Interval (S_1, Δu_c) denote the procedure that generates the uniformly distributed $S_i's$ corresponding to a given S_1 and Δu_c, we adopt a simple dual-direction bi-section approach to calculate Δu_c, as outlined below.

Obviously, setting Δu_i to be a constant tends to be conservative, albeit the nice uniformity pattern of front curves. As an improvement, sequential maximization tries to maximize Δu_i for every i, starting from the first uv-front curve S_1.

Procedure **Calculate_Uniform_Interval**

Input: three valuables t_0, t_1 and u_0.

Output: the constant parameter interval Δu_c.

$iter \leftarrow 1$, $\theta_{max}^0 \leftarrow \theta_s$ // initialization

$\Delta u_1 \leftarrow 0$

$\Delta u_2 \leftarrow 1 - u_0$

$S_1 = \mathbf{Front\_Curve}(t_0, t_1, u_0)$

$\{S_2, S_3, \ldots\} = \mathbf{Propagation\_Constant\_Interval}\ (S_1, \frac{\Delta u_1 + \Delta u_2}{2})$

Calculate θ_{i_max} between $r(S_i)$ and $r(S_{i+1})$ for i = 1, 2, …, N-1.

$\theta_{max}^{iter} = \boldsymbol{max}\ \{\theta_{1\_max}, \theta_{2\_max}, \ldots\}$

while $\left|\theta_{max}^{iter} - \theta_{max}^{iter-1}\right| < \delta$ // δ is a given tolerance

if $\theta_{max}^{iter} \geq \theta_s$

$\Delta u_2 \leftarrow \frac{\Delta u_1 + \Delta u_2}{2}$

end if

if $\theta_{max}^{iter} < \theta_s$

$\Delta u_1 \leftarrow \frac{\Delta u_1 + \Delta u_2}{2}$

end if

$iter \leftarrow iter + 1$

$\{S_2, S_3, \ldots\} =$**Propagation_Constant_Interval** $(S_1, \frac{\Delta u_1 + \Delta u_2}{2})$

Calculate θ_{i_max} between $r(S_i)$ and $r(S_{i+1})$ for i = 1, 2, …, N-1.

$\theta_{max}^{iter} = \boldsymbol{max}\ \{\theta_{1\_max}, \theta_{2\_max}, \ldots\}$

end while

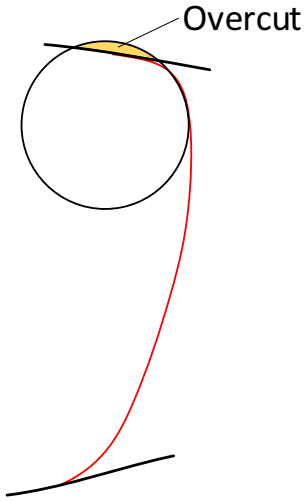

Fig. 7 The occurrence of overcut at the boundary of the slot

3.1.2 Sequential maximization of Δu_i

Basically, given an S_i, we can increase the displacement Δu_i as much as possible until the angle θ_{i_max} reaches the threshold θ_s. In our implementation, we use a variant of Newton's iterative method to find the Δu_i that realizes the equality $\theta_{i\_max} = \theta_s$ (details omitted). Therefore, given the first *uv*-front curve S_1, we can sequentially generate the following ones S_2, S_3, ..., until the last one S_N, and be ascertained that, except for perhaps the last chip between $r(S_{N-1})$ and $r(S_N)$, for every pair of $r(S_i)$ and $r(S_{i+1})$, the angle θ_{i_max} is maximized to be θ_s. Though by nature this is only a local optimization, our preliminary tests have shown that in many cases, it fares very close to the global optima (obtained in our tests by exhaustive search).

3.2 Formulation of the optimization

Regardless of uniform or sequentially maximized Δu_i, as long as the first *uv*-front curve S_1 is given, the rest of the *uv*-front curves $\{S_2, S_3, \ldots, S_N\}$ are fully determined. As S_1 is determined by the three parameters $\{u_0, t_0, t_1\}$ (see Fig. 4a), they become the variables of our optimization problem. Referring to Fig. 2, let T_i denote the corresponding tool path of the front curve F_i, which is essentially the offset of F_i with the tool radius R_s. Assuming a constant feed rate, the cutting time of T_i can then be represented by its length, i.e., l_i. Thus, for any trio $\{u_0, t_0, t_1\}$, there is a corresponding total length of the cutting tool paths, i.e., $L_t(u_0, t_0, t_1) = \sum_i l_i$. The following formulation of optimization is then in order:

$$\begin{aligned} obj &: min\ \{L_t(u_0, t_0, t_1)\} \\ s.t. &: R_{min} > R_s \end{aligned} \tag{4}$$

where R_{min} stands for the smallest radius of curvature on any front curve F_i. The constraint $R_{min} > R_s$ must be respected due to two obvious reasons: (1) a tool of radius R_s can never cut out a front curve of curvature larger than $1/R_s$; and (2) even if we ignore this physical infeasibility (as T_i is a self-intersection-removed offset of F_i), we must not allow the violation $R_{min} < R_s$ to occur near the two ends of the front curve, for otherwise overcut would happen at the boundary of the slot, as illustrated in Fig. 7.

Finally, about the specific optimization technique for solving Eq. (4), in the current implementation, we use the Genetic Algorithm, although other popular ones such as the Particle Swarm Optimization may well suit our need.

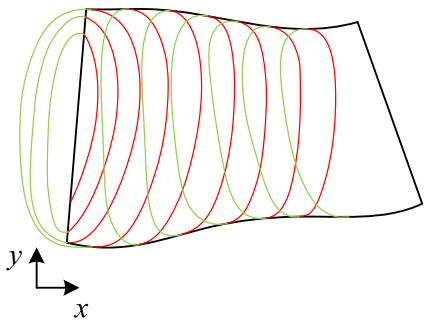

Fig. 8 Active front curves (red) and non-active connection curves (green)

4 Experimental results

A prototype of the proposed method has been implemented by us in MATLAB. To compare the proposed new trochoidal milling pattern with the traditional circular trochoidal milling, several freeform slots are selected for simulation tests, as well as one physical cutting test. For all the tests, the engagement angle threshold θ_s is set at 100°.

Before reporting the test results though, it is necessary to mention the non-active part on a tool path. As milling is a continuous cutting process, the tool paths $T_1, T_2, \ldots, T_{N-1}$ must be connected together. Specifically, the end point of the front curve F_i must be at least C^1 continuously connected to the start point of the next front curve F_{i+1} by some smooth curve, e.g., the green ones in Fig. 8. These connection curves are said to be *non-active* (i.e., non-cutting) since, except near their end points, the corresponding tool does not cut the material. In our implementation, these connection curves are also defined as cubic splines, which are easy to adjust. Because they are non-active, they could be adjusted to be short, as long as the tangent continuity at the ends is ensured. Once these connection curves are defined, their corresponding tool paths can be readily obtained by means of offsetting, resulting in a single and C^1 continuous tool path for milling the entire slot. As indicated in Eq. (4), only the active cutting tool path is considered in the efficiency calculation, while the non-active part is usually assigned with a much faster feed rate and is thus negligible compared to the active part.

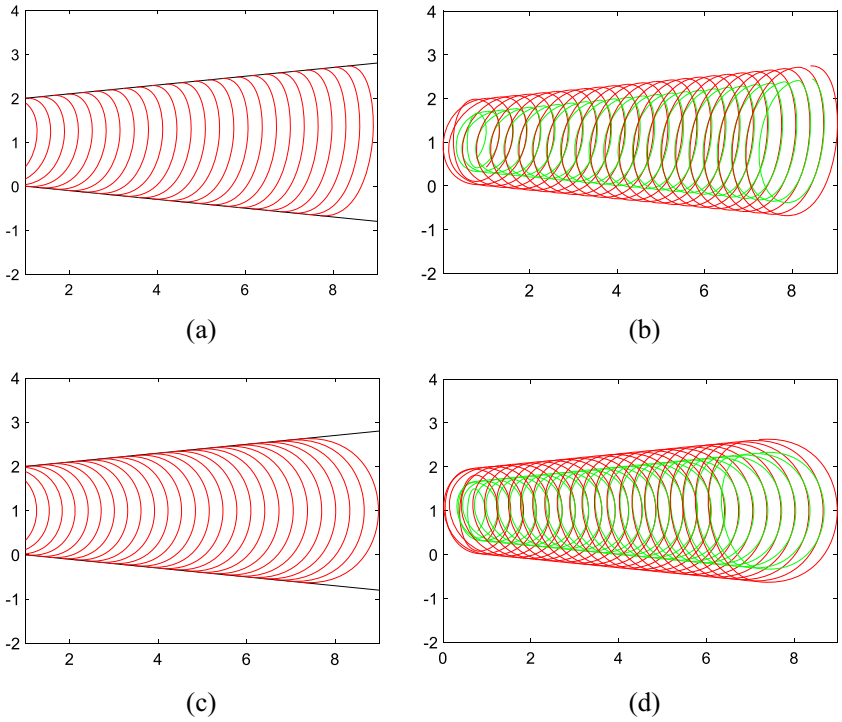

Fig. 9 **a**, **b** The proposed trochoidal tool path, total active tool path length is 63.32 units. **c**, **d** The traditional circular trochoidal milling, total active tool path length is 84.48 units; efficiency improvement = 25% (cutter radius = 0.3 units)

For the first simulation test, three cutters with radius 0.3, 0.4, and 0.5 units were selected and tested on a simple cone-shaped slot, while sequentially maximized Δu_i's were used. The simulation results are shown in Figs. 9, 10, and 11, where the red curves are the generated front curves and their connection curves and the green ones are the corresponding tool paths (in the left column, only active front curves are shown).

The test data from Figs. 9, 10, and 11 clearly indicate that the efficiency improvement of ours over the traditional trochoidal milling increases with the decrease of the tool radius. That is, the proposed trochoidal milling pattern is more

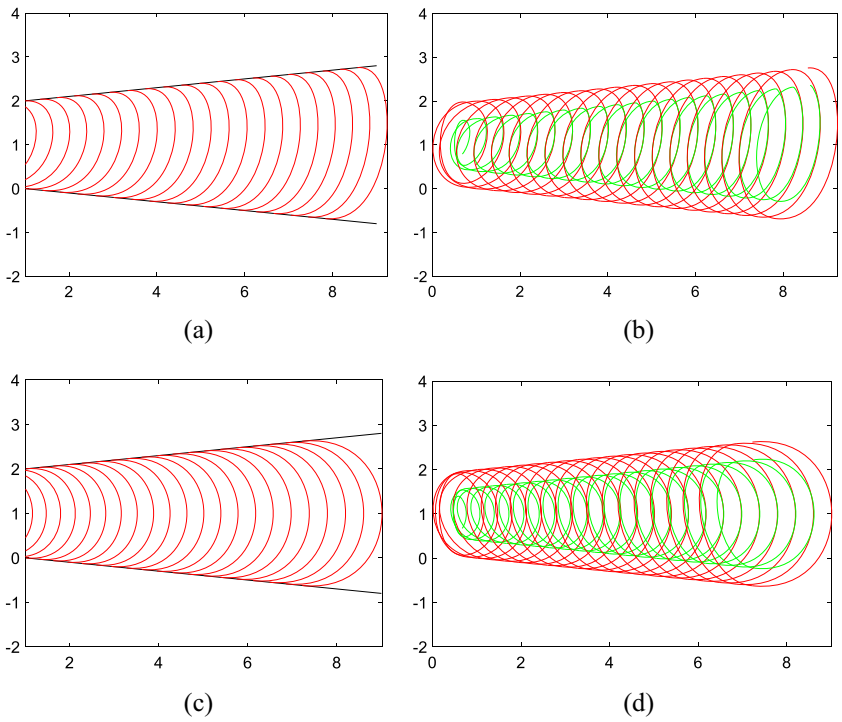

Fig. 10 **a**, **b** The proposed trochoidal tool path, total active tool path length is 49.34 units. **c**, **d** The traditional circular trochoidal milling, total active tool path length is 62.24 units; efficiency improvement = 20.73% (cutter radius = 0.4 units)

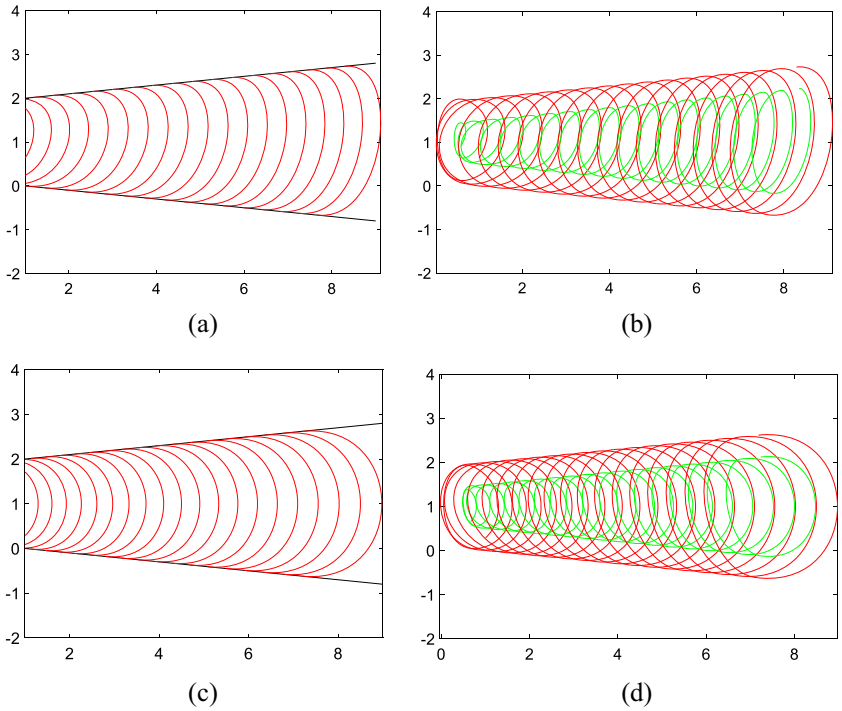

Fig. 11 **a**, **b** The proposed trochoidal tool path, total active tool path length is 41.08 units. **c**, **d** The traditional circular trochoidal milling, total active tool path length is 50.11 units; efficiency improvement = 18.02% (cutter radius = 0.5 units)

effective when a smaller tool is used. However, a smaller tool always leads to a longer tool path length and hence a longer machining time, in addition to other limiting factors such as a smaller feed rate and lower stiffness of the tool. Therefore, a trade-off is required.

As a validation of efficiency enhancement by our method, for the case of cutter radius = 0.3 units, Fig. 12 shows the varying cutter-workpiece engagement angle of the front curves of our tool path vs. the traditional circular trochoidal tool path. The curves in Fig. 12 represent the engagement changing situation of cutter in every trochoidal cutting path, as many cutting paths are needed for machining one slot. The change of color of curves from red to blue indicates the sequence of the corresponding front curve during the process. The pure red curve identifies the engagement changing situation of the first trochoidal cutting path while the pure blue curve the final trochoidal cutting path. As evidently seen in Fig. 12a, b, while in both tool paths, the maximum engagement angle is capped under the given 100° threshold, ours tried to push the average upward. As the material removal rate (MRR) is positively related to the engagement angle, a larger average of engagement angle indicates a faster MRR, thus a shorter total machining time.

From now on, for the rest of the tests, the cutter radius is set to be 0.3 units and θ_s remains to be 100°.

The results of the second simulation test are given in Fig. 13. As revealed from the figure, this time, the outcome of uniform distribution of front curves did not fare very well (achieving almost zero reduction in total machining time over the traditional one), while the sequential maximization approach achieved a reduction of 12.2%.

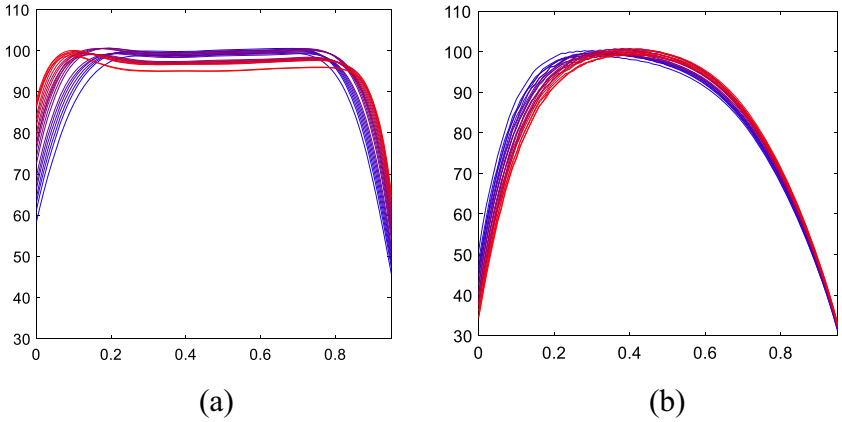

Fig. 12 The cutter-workpiece engagement angle of our new trochoidal tool path (**a**) and the traditional circular trochoidal tool path (**b**) of simulation test 1 (cutter radius = 0.3 units)

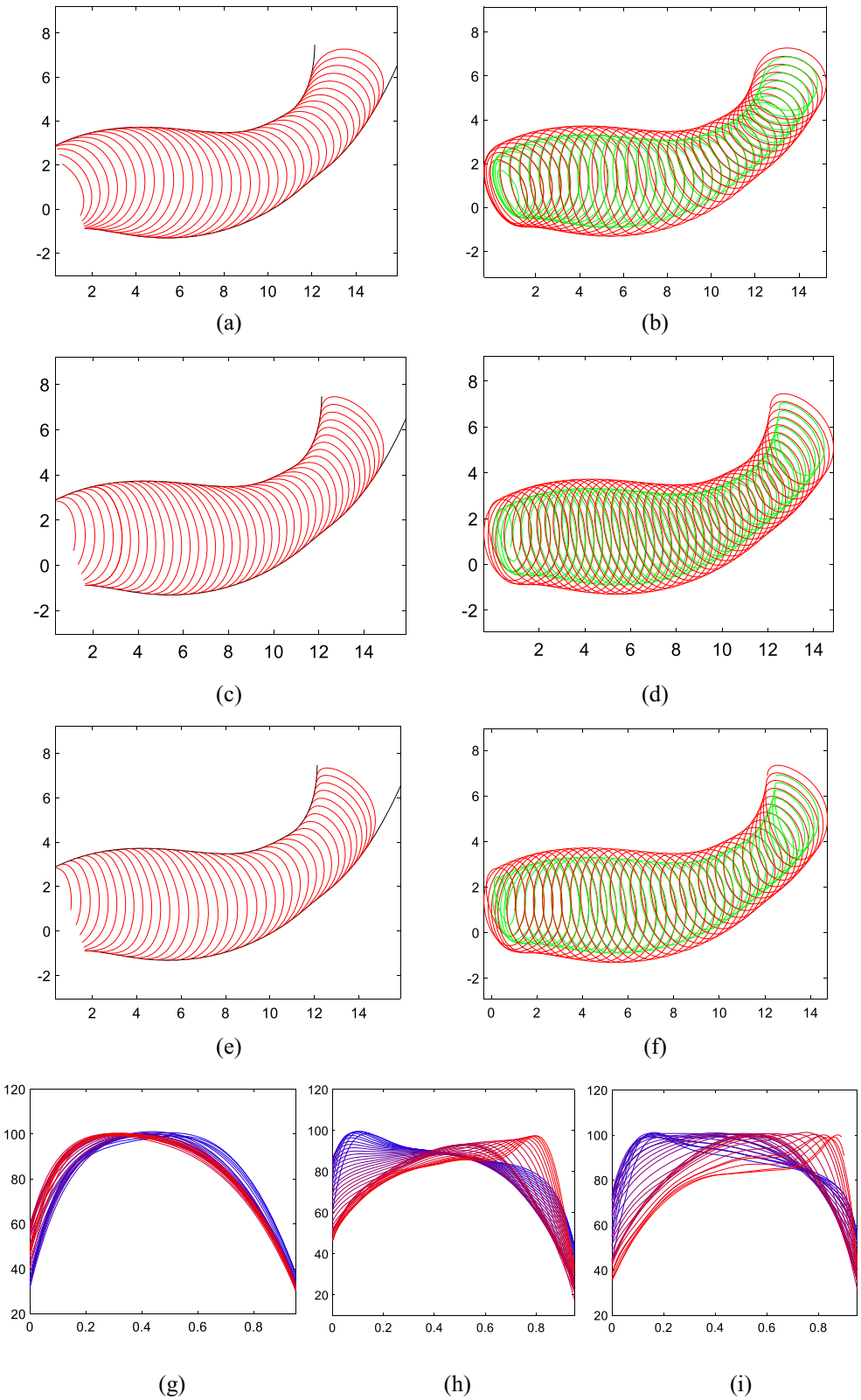

Fig. 13 **a**, **b** The traditional circular trochoidal milling, total active tool path length is 182.88 units. **c**, **d** The proposed trochoidal tool path, uniform Δu_i, total active tool path length is 181.82 units. **e**, **f** The proposed trochoidal tool path, sequentially maximized Δu_i, total active tool path length is 160.58 units. **g**–**i** The engagement angle of **a**, **b**, **c**, **d**, and **e**, **f**, respectively

Figure 14 shows the results of our last test. The same shape of the slot was also used by Wang et al. [20] in their test using the traditional trochoidal milling method. This time, our new trochoidal tool path (using the sequentially maximized Δu_i) enjoys a commanding 26% reduction in total machining time over the traditional one.

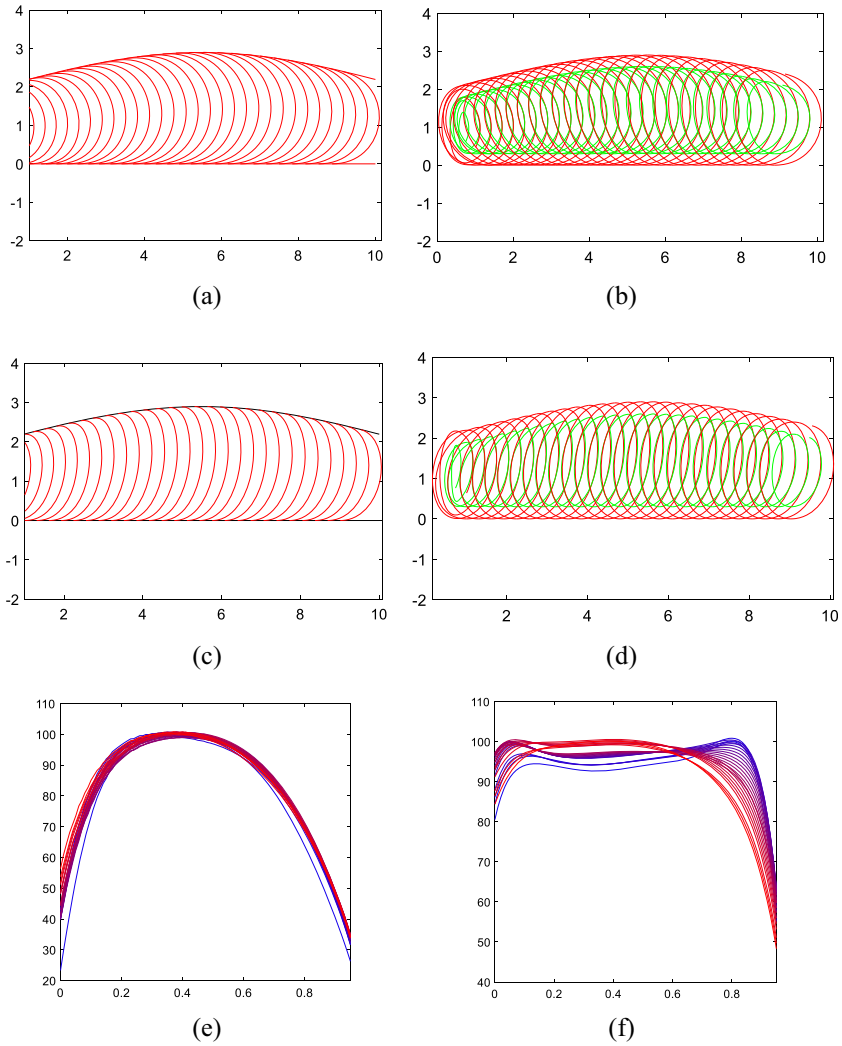

Fig. 14 **a**, **b** The traditional circular trochoidal milling, total active tool path length is 92.74 units. **c**, **d** The proposed trochoidal tool path, sequentially maximized Δu_i, total active tool path length is 68.59 units. **e**, **f** The engagement angle of **a**, **b** and **c**, **d**, respectively

Finally, as a further validation of our work, we also performed a physical cutting experiment using the two tool paths from the last simulation test, i.e., Fig. 14. The material to cut was Bakelite; the spindle speed was set at 8000 rpm; and the feed rate of the active cutting part of tool paths was 500 mm/min, while that for the no-cutting part was coded with the rapid transit command in the final G-code program. The total time of slotting taken by the traditional method is 132 s, while that taken by ours is only 99 s, a reduction of 25%, which finds a good agreement with the simulation result of 26%. The finally machined slots are shown in Fig. 15.

5 Conclusion

Traditional circular type trochoidal milling is a popular strategy for slotting operation, as it avoids the full cutter-workpiece engagement and hence prolongs the tool service life. However, its drawback is also obvious, as within each trochoidal cycle, the engagement angle reaches the maximum only in the middle position and its average value is low, which significantly drags down the material removal rate. To address this issue, in this paper, we have proposed a new type of trochoidal pattern for milling an arbitrary slot with a curved boundary and non-constant width. By means of finding a suitable basic shape

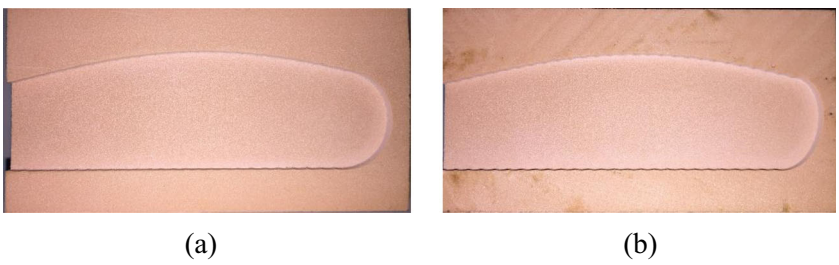

Fig. 15 The physically machined slots using the tool paths from the last simulation test (i.e., Fig. 14): **a** by the traditional trochoidal tool path and **b** by our new trochoidal tool path (using the sequentially maximized Δu_i)

of the front curve and then adaptively maximizing the step-over distance between consecutive front curves, a higher average of engagement angle can be achieved (but still under the specified threshold on the maximum), thus raising the material removal rate and shortening the total machining time accordingly. As expected, the improvement in machining efficiency by our new type over the traditional one becomes more prominent with the decrease of the cutter radius, which has also been confirmed by our simulation tests.

The future work in this subject may focus on several aspects. First, in this work, the sole constraint on the step-over distance is the threshold on maximum engagement angle, which indeed is critical. Nonetheless, there could be other types of constraints that need to be considered, such as the avoidance of chattering which is related to not only the step-over distance but also the feed rate. Secondly, our current optimization algorithm is rather simplistic (even with the sequentially maximized step-over distance); we ought to ask if a more elaborated one could be developed. Finally, we will explore possible applications of the proposed type of trochoidal pattern to other areas in manufacturing, not limited to only the slotting operation.

References

1. Kim H-C (2007) Tool path modification for optimized pocket milling. Int J Prod Res 45:5715–5729. https://doi.org/10.1080/00207540600919340
2. Wang ZG, Rahman M, Wong YS (2005) Tool wear characteristics of binderless CBN tools used in high-speed milling of titanium alloys. Wear 258:752–758. https://doi.org/10.1016/j.wear.2004.09.066
3. Rauch M, Duc E, Hascoet J-Y (2009) Improving trochoidal tool paths generation and implementation using process constraints modelling. Int J Mach Tools Manuf 49:375–383. https://doi.org/10.1016/j.ijmachtools.2008.12.006
4. Otkur M, Lazoglu I (2007) Trochoidal milling. Int J Mach Tools Manuf 47:1324–1332. https://doi.org/10.1016/j.ijmachtools.2006.08.002
5. Ibaraki S, Yamaji I, Matsubara A (2010) On the removal of critical cutting regions by trochoidal grooving. Precis Eng 34:467–473. https://doi.org/10.1016/j.precisioneng.2010.01.007
6. Zhao ZY, Wang CY, Zhou HM, Qin Z (2007) Pocketing toolpath optimization for sharp corners. J Mater Process Technol 192-193:175–180. https://doi.org/10.1016/j.jmatprotec.2007.04.096
7. Deng Q, Mo R, Chen ZC, Chang Z (2018) A new approach to generating trochoidal tool paths for effective corner machining. Int J Adv Manuf Technol 95:3001–3012. https://doi.org/10.1007/s00170-017-1353-3
8. Choy HS, Chan KW (2003) A corner-looping based tool path for pocket milling. Comput Aided Des 35:155–166. https://doi.org/10.1016/S0010-4485(02)00049-0
9. Pleta A, Mears L (2016) Cutting force investigation of Trochoidal milling in nickel-based Superalloy. Procedia Manuf 5:1348–1356. https://doi.org/10.1016/j.promfg.2016.08.105
10. Pleta A, Ulutan D, Mears L. Investigation of Trochoidal milling in nickel-based Superalloy Inconel 738 and comparison with end milling. In: ASME 2014 International Manufacturing Science and Engineering Conference collocated with the JSME 2014 International Conference on Materials and Processing and the 42nd North American Manufacturing Research Conference; Monday 9 June 2014; Detroit, Michigan, USA: ASME; Monday 9 June 2014. V002T02A058. https://doi.org/10.1115/MSEC2014-4151
11. Wu BH, Zheng CY, Luo M, He XD (2012) Investigation of Trochoidal milling nickel-based Superalloy. MSF 723:332–336. https://doi.org/10.4028/www.scientific.net/MSF.723.332
12. Ferreira JCE, Ochoa DM (2013) A method for generating trochoidal tool paths for 2½D pocket milling process planning with multiple tools. Proc Inst Mech Eng B J Eng Manuf 227:1287–1298. https://doi.org/10.1177/0954405413487897
13. Elber G, Cohen E, Drake S (2005) MATHSM: medial axis transform toward high speed machining of pockets. Comput Aided Des 37:241–250. https://doi.org/10.1016/j.cad.2004.05.008
14. Yamaji I, Ibaraki S, Kakino Y, Nishida S. (2003) Tool path planning using trochoid cycles for hardened steel in die and mold manufacturing (2nd report) – tool path planning to avoid an excessive tool load –. In: Proceedings of the int. conference on agile manufacturing. pp 443–50. https://www.researchgate.net/profile/Soichi_Ibaraki/publication/242675660_Tool_Path_Planning_Using_Trochoid_Cycles_for_Hardened_Steel_in_Die_and_Mold_Manufacturing_2_nd_Report_Tool_Path_Planning_to_Avoid_an_Excessive_Tool_Load/links/59a7609c0f7e9b41b7892650/Tool-Path-Planning-Using-Trochoid-Cycles-for-Hardened-Steel-in-Die-and-Mold-Manufacturing-2-nd-Report-Tool-Path-Planning-to-Avoid-an-Excessive-Tool-Load.pdf. Accessed 20 Jun 2018
15. Pleta A, Niaki FA, Mears L (2017) Investigation of Chip thickness and force modelling of Trochoidal milling. Procedia Manuf 10:612–621. https://doi.org/10.1016/j.promfg.2017.07.063
16. Kardes N, Altintas Y (2007) Mechanics and dynamics of the circular milling process. J Manuf Sci Eng 129:21. https://doi.org/10.1115/1.2345391
17. Baskar N, Asokan P, Prabhaharan G, Saravanan R (2005) Optimization of machining parameters for milling operations using non-conventional methods. Int J Adv Manuf Technol 25:1078–1088. https://doi.org/10.1007/s00170-003-1939-9
18. Mestry, Tushar, and Niyati Raut. Optimization of Cutting Parameters in High Speed Trochoidal Machining. http://ijiset.com/vol4/v4s4/IJISET_V4_I04_24.pdf. Accessed 20 Jun 2018
19. Yan R, Li H, Peng F, Tang X, Xu J, Zeng H (2017) Stability prediction and step optimization of Trochoidal milling. J Manuf Sci Eng 139:91006. https://doi.org/10.1115/1.4036784
20. Wang Q-H, Wang S, Jiang F, Li J-R (2016) Adaptive trochoidal toolpath for complex pockets machining. Int J Prod Res 54:5976–5989. https://doi.org/10.1080/00207543.2016.1143135
21. Salehi M, Blum M, Fath B, Akyol T, Haas R, Ovtcharova J (2016) Epicycloidal versus Trochoidal milling-comparison of cutting force, tool tip vibration, and machining cycle time. Procedia CIRP 46:230–233. https://doi.org/10.1016/j.procir.2016.04.001
22. Li S, Wang X, Xie L, Pang S, Peng S, Liang Z, Jiao L (2015) The milling–milling machining method and its realization. Int J Adv Manuf Technol 76:1151–1161. https://doi.org/10.1007/s00170-014-6345-y